Electric fatigue in antiferroelectric ceramics induced by bipolar electric cycling

Longjie Zhou[a)]
Max-Planck-Institut für Metallforschung and Institut für Nichtmetallische Anorganische Materialien, Universität Stuttgart, Pulvermetallurgisches Laboratorium, Heisenbergstrasse 3, 70569 Stuttgart, Germany

R. Z. Zuo
Institute of Materials Science, Darmstadt University of Technology, Petersenstrasse 23, 64287 Darmstadt, Germany

G. Rixecker and A. Zimmermann[b)]
Max-Planck-Institut für Metallforschung and Institut für Nichtmetallische Anorganische Materialien, Universität Stuttgart, Pulvermetallurgisches Laboratorium, Heisenbergstrasse 3, 70569 Stuttgart, Germany

T. Utschig
Institute of Materials Science, Darmstadt University of Technology, Petersenstrasse 23, 64287 Darmstadt, Germany

F. Aldinger
Max-Planck-Institut für Metallforschung and Institut für Nichtmetallische Anorganische Materialien, Universität Stuttgart, Pulvermetallurgisches Laboratorium, Heisenbergstrasse 3, 70569 Stuttgart, Germany

(Received 19 January 2005; accepted 16 January 2006; published online 17 February 2006)

The fatigue behavior of antiferroelectric lanthanum-doped lead zirconate stannate titanate bulk material induced by bipolar cycling was investigated. Strain and polarization hysteresis loops, acoustic emissions (AEs), and biaxial strength were monitored. The material showed a high resistance to electric fatigue, concerning the losses in maximum strain, switchable polarization, and biaxial strength as well as modifications of AE patterns and microstructure. Fatigue microcracking is weak in the material during cycling. The pinning of antiferroelectric and ferroelectric domains by point defect agglomeration is discussed as the main fatigue mechanism. A diffuse antiferroelectric-ferroelectric phase transition and an asymmetry of the strain hysteresis loop due to the electric cycling are described and explained as a result of the pinning process and offset polarization. © *2006 American Institute of Physics*. [DOI: 10.1063/1.2172725]

I. INTRODUCTION

Antiferroelectric (AFE) materials have received increasing attention due to their potential usage as microactuators and energy storage capacitors.[1,2] Bulk materials and thin films of lanthanum-doped lead zirconate stannate titanate (PZST) and further modified forms are of particular interest, since on the one hand there is a large electrically induced longitudinal strain due to the phase transition from the tetragonal antiferroelectric to the rhombohedral ferroelectric (FE) phase in materials composed close to the morphotropic phase boundary between the antiferroelectric and ferroelectric phases.[3,4] On the other hand, the field forced ferroelectrics release all polarization charges and therefore can supply very high instantaneous current at the inversion of the phase transition, from FE to AFE state.[5,6] However, like ferroelectric materials, the antiferroelectric PZST ceramics show electric fatigue effect at high a c fields, which has been mechanically and electrically the major hindrance for applications of the materials so far.[7,8]

The electric fatigue of ferroelectric and antiferroelectric materials is referred to the gradual decrease of switchable or remanent polarization and of the corresponding field induced strain under a c fields.[9] The fatigue phenomenon in those ceramics has been attracting the interest of many researchers for more than a decade due to the large market shares to be gained with nonfatiguing ferroelectric memories and multilayer actuator components.[10] Fatigue effects can be initiated by numerous factors, including intrinsic characteristics of the materials and extrinsic contributions. Intrinsic characteristics are the composition and the microstructure of the bulk materials or thin films; extrinsic contributions include surface condition, electrodes, and temperature as well as the frequency, strength, and type of driving field. There have been numerous models concerning the mechanisms of electric fatigue, including those of electrochemical variations and mechanical deterioration.[11] The former is based on the scenario that domains become inactive due to point defects pinning the domain walls.[12–14] The latter rests on the hypothesis that microcracks reduce the local effective field or yield conductive corrosion pathways in the material, thus decreasing the number of domains which switch in the proximity of such cracks.[15,16] The electrochemical variations can be relieved to some extent by heat treatment at 300–500 °C,[17] while the mechanical deterioration in fatigued samples cannot be recovered below sintering temperatures.

[a)]Author to whom correspondence should be addressed; electronic mail: zhou@mf.mpg.de
[b)]Present address: Robert Bosch GmbH, Corporate Research and Development.

The above-mentioned results concerning fatigue phenomena, factors relevant for the effect, and fatigue mechanisms are mostly based on the investigations on ferroelectrics rather than antiferroelectrics thus the study of antiferroelectric fatigue is inadequate so far. Nevertheless, all of the researches on antiferroelectric fatigue showed that the materials exhibit higher fatigue resistance than ferroelectric ones. It was summarized in a previous paper that general agreement had been reached that the amplitude of switchable polarization in ferroelectric materials decreases to around 20%–30% of the original value when the cycle number approaches 10^8.[10] Antiferroelectric ceramics show much less loss in polarization than ferroelectric ones at similar driving conditions and cycle number.[18–20] Four stages of electric fatigue in ferroelectrics under bipolar cycling have been identified, including an incubation period, a stage of logarithmic fatigue, a saturation regime, and a recovery stage.[11,21] The final stage reaches to 10^8 cycles. Those four fatigue stages have not been fully revealed in antiferroelectrics for the cycle numbers up to 10^9.[18] The higher fatigue resistance of antiferroelectric ceramics was attributed to the different mechanism of the switching of polarization as compared to ferroelectric ceramics. Switching in antiferroelectrics involves the AFE-FE phase transition, where the polarization direction changes by 180° with the consequence of smaller internal stresses than those generated by switching the spontaneous polarization of the ferroelectrics by 90°.[18,19]

Acoustic emission (AE) has been widely used as a nondestructive test (NDT) to monitor dynamic processes in materials.[22] Generally, the acoustic emission method detects all abrupt local stress or strain changes within a material.[23] The method was reported to identify microscopic modifications and damage in ferroelectric materials, such as ceramics, single crystals, and devices, but not yet in antiferroelectric materials. Possible acoustic emission sources in ferroelectric ceramics are microcracking, discontinuous switching, crystallographic phase transformation, internal discharges in pores or microcracks, or surface friction of the macroscopic sample.[24]

The AE method, combined with measurements of strain and polarization hysteresis loops, was applied in one instance to evaluate damage and fatigue effect in ferroelectric PZT materials.[11] A similar study to reveal electric fatigue in antiferroelectric material has not been reported so far. Mechanical strength as a function of electric cycling is of much technological importance to actuators but was rarely reported previously as well. The present study intends to combine those approaches as well as mechanical strength measurements to investigate fatigue effects in antiferroelectric PZST ceramics.

II. EXPERIMENT

A. Sample preparation

The composition of the antiferroelectric material investigated in this study was $Pb_{0.97}La_{0.02}(Zr_{0.55}Sn_{0.33}Ti_{0.12})O_3$. Samples were prepared by solid-state reactions and conventional sintering, using reagent-grade raw oxides as starting materials. The starting oxides were mixed and attrition milled in isopropanol with small zirconia balls as milling media in order to increase their reactivity and to get highly intimately mixed materials. After drying, the mixtures were calcined at 850 °C for 5 h and attrition milled again. The resulting powder was cold isostatically pressed at 200 MPa into disk-shaped compacts, which were then sintered at 1150 °C for 2 h and at 1250 °C for additional 2 h in a PbO-rich oxygen atmosphere, followed by an annealing at 500 °C for 8 h to release internal stress of the specimens. The samples were ground into thin disks, 10 mm in diameter and 0.4 mm in thickness, with flat and parallel major surfaces, followed by polishing to a 1 μm finish and fully sputtering with gold electrodes.

B. Electric cycling

The maximum value of the bipolar cycling field was chosen as 4 kV/mm, which is 1.5 kV/mm higher than the antiferroelectric to ferroelectric transition field (2.5 kV/mm). An electric transmitter provided the required sinusoidal voltage (50 Hz) from the normal electric line voltage. The voltage could be regulated between zero and maximum value. The cycling field was slowly and steadily increased and decreased when loading and unloading. Six samples were used as one batch for cycling. The samples were immersed in a bath of silicone oil in order to avoid arcing and to ensure good heat transfer. The maximum temperature of the silicone oil is no more than 40 °C during the electric cycling. The cycle numbers for the individual batches of samples were selected as $10^{4.5}$, 10^5, $10^{5.5}$, 10^6, $10^{6.5}$, 10^7, $10^{7.25}$, $10^{7.5}$, $10^{7.75}$, 10^8, and 1.2×10^8 cycles. The property measurements were conducted on the samples after cycling.

C. Measurements

The setup for the measurement of strain hysteresis loop, polarization hysteresis loop, and AE pattern was described in details in a previous paper.[11] For strain hysteresis loops, a linear variable displacement transducer (LVDT, resolution: 20 nm) connected to an ac measuring bridge (Hottinger Baldwin Meßtechnik, Darmstadt, Germany) was used. The polarization hysteresis loops were determined by a linear capacitor ($C=4.49\ \mu F \gg C_{sample}$) placed between the sample and ground. The voltage U on this capacitor was measured by an electrometer (Keithley Instruments, Cleveland, OH, USA) and converted to polarization. A commercial AE-detection device of bandwidth of 100–2000 kHz (AMS3, Vallen Systeme, Icking, Germany) was used. The amplification was chosen as 49 dB, and the threshold as 30.2 dB. The amplitude scale (in decibel) is given with respect to 3.5 μV. Amplitude maxima were recorded for each AE event. A high-voltage source of very narrow bandwidth near dc was used to reduce spurious electromagnetic noise, and the damping was further enhanced by a *RC*-low pass filter. A bipolar triangular measuring field was driven to a maximum value of 4 kV/mm at 0.02 Hz for the measurement. This bipolar cycle was applied thrice for each measurement. All data (polarization, field, strain, and AE) were simultaneously recorded by the measuring setup. To avoid arcing, the samples

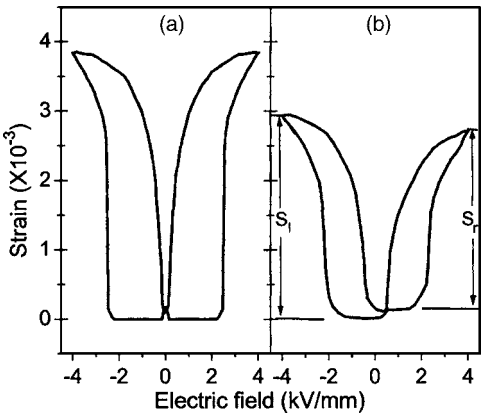

FIG. 1. Strain hysteresis loops for the material in (a) the virgin state and (b) the fatigued state (cycled at 4 kV/mm, 50 Hz for 10^8 cycles).

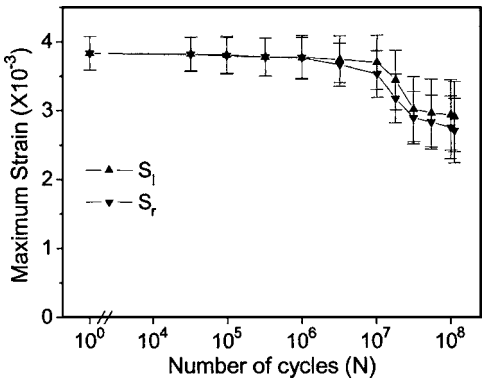

FIG. 2. The maximum strain of the left (S_l) and right (S_r) side of the strain hysteresis loop as a function of cycling.

were placed in a silicone oil bath, which also provided the acoustical contact. For some samples, the measurements were also conducted after a heat treatment at 500 °C for 1 h. For the electric cycling and the measurements, the difference in the temperature of the samples is less than 20 °C and the driving frequencies in both cases are rather low, it is expected that the responses of the field induced strain and polarization to both driving conditions are similar.

Biaxial strength was measured by the ball-on-three-balls test, which is suitable for the geometry of the samples. In the test, a disk sample is supported by three balls and then axially loaded form the opposite side via a fourth ball. The calculation of the biaxial strength is based on a finite element (FE) analysis of the stress state in a loaded disk. The maximum tensile stress, $\sigma_{\max}$, scales with the applied force F, and with the inverse square of the thickness of the sample t,

$$\sigma_{\max} = f \cdot F/t^2, \tag{1}$$

where the factor f is a dimensionless function of the ratio of the support radius R_a to the sample radius R, the ratio of the sample thickness t to the radius R, and Poisson's ratio of the sample ν. For more in details about the test, refer to Ref. 25.

The microstructure of the major surfaces of the fatigued samples was observed by optical microscopy (Leica DM RM, Leica Microsystems AG, Germany) after the electrodes had been removed, and by scanning electron microscopy (SEM, JEOL 6300F) after etching of the surface. A solution of 5 ml of HCl and 95 ml of distilled water, containing a few drops of HF acid, was used as etchant. A few seconds of exposure gave clear images of the grains. The microstructure of fracture surfaces of the specimens was observed by the SEM. The virgin samples were observed in an identical way as references.

III. EXPERIMENTAL RESULTS

Results of macroscopic properties, AE measurement, and microstructure for the material undergoing the electric cycling are presented below to reveal the fatigue effect.

A. Strain hysteresis loop

The strain hysteresis data were taken from the center of the samples. Figure 1 shows strain hysteresis loops for the virgin material and for the fatigued material after 10^8 cycles. For the virgin material, a higher electric field is needed to drive the first AFE-FE phase transition. The loop for the virgin material shown in the figure is that of the second measurement cycle. The virgin loop is typical for antiferroelectric bulk materials, showing a normal phase transition (NPT) with a clearly defined transition field (E_{AF}) of 2.5 kV/mm and a sudden increase in strain at that field. Compared with the virgin one, the fatigued loop exhibits an asymmetric decrease and a diffuse AFE-FE phase transition (DPT) characterized by the fact that the AFE-FE phase transition takes place in a range rather than at a particular value of the electric field. The asymmetry is caused by two different phenomena. First, the whole loop is shifted to the right into the electric positive direction. Secondly, the maximum strain observed in the left wing (S_l) of the hysteresis loop is higher than in the right wing (S_r).

For each cycled sample the strain hysteresis loop exhibits an asymmetry always in the same direction. The decrease in maximum strain and the extent of the asymmetry as well as the diffuse character of the AFE-FE phase transitions show an increasing trend with cycle number. S_l and S_r as a function of cycle number are provided in Fig. 2. The extent of the diffuseness of the phase transition cannot be quantified so far.

B. Polarization hysteresis loop

Figure 3 displays polarization hysteresis loops corresponding to the strain hysteresis loops shown in Fig. 1 for the virgin and fatigued materials. The virgin loop is also that of the second measurement cycle. Compared with the virgin one, the polarization hysteresis loop for the fatigued material shows a decrease in the amplitude of switchable polarization (P_s). The diffuse character of the AFE-FE phase transition is also characterized in the fatigued polarization loop by a more gradual increase of the polarization within a larger range of electric field. As a result, the fatigued loop shows a less square shape. Figure 4 shows the decreasing values of P_s as a function of cycle number.

C. Acoustic emission

The amplitude spectra as a function of the applied field, corresponding to the strain and polarization hysteresis loops

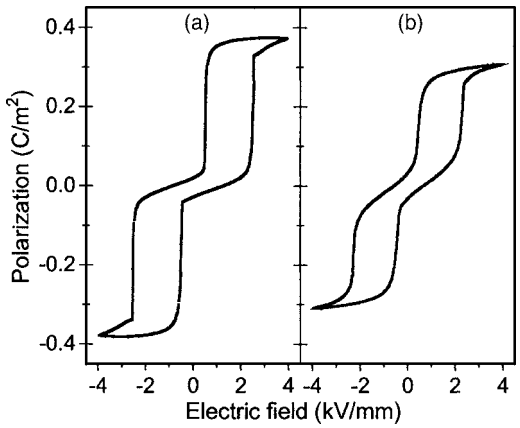

FIG. 3. Polarization hysteresis loops for the material in (a) the virgin state and (b) the fatigued state (cycled at 4 kV/mm, 50 Hz for 10^8 cycles).

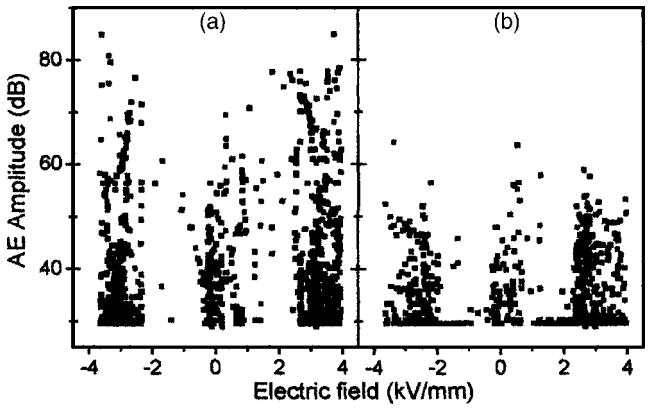

FIG. 5. AE patterns corresponding to hysteresis loops for the samples in (a) the virgin state and (b) the fatigued state (cycled at 4 kV/mm, 50 Hz for 10^8 cycles).

of Figs. 1 and 2 for virgin and fatigued samples, are shown in Fig. 5. Time dependent AE patterns are plotted in Fig. 6. Each data point represents one single AE event. For the virgin samples, on the increasing electric field a few AE events occur below the AFE-FE transition field. Just around E_{AF} numerous AE events of different amplitudes appear and continue to take place while until the maximum applied field (E_{max}) of 4 kV/mm is reached. For decreasing electric field, numerous AE occur only around E_{FA}. The AE patterns for the fatigued samples are similar to those of the virgin one. The maximum and average amplitudes of the AE hits in a measurement cycle decrease with the number of cycles, i.e., from 85 to 42 dB in the unfatigued state to 65 and 35 dB after 10^8 cycles, respectively. The number of AE events during a measuring cycle remains unchanged on the order of 10^3, independent of the number of cycles.

D. Biaxial strength and microstructure

The biaxial strength of the material as a function of the number of cycles is plotted in Fig. 7. The material shows a high resistance of mechanical strength to the bipolar cycling. The strength shows a only slightly decreasing trend, with significant losses occurring at high cycle numbers only. After 10^8 cycles, the biaxial strength has decreased by 15% of its original value.

No significant difference was observed in the microstructure of the polished major surfaces of the virgin sample and the sample that suffered 10^8 cycles by using optical microscopy. There were no macro- and microcracks noticeable on the polished surfaces. After chemical etching, the virgin sample exhibits undamaged grains [Fig. 8(a)], while numerous etch grooves within grains can be found in the microstructure of the fatigued sample [Figs. 8(b) and 8(c)]. No identical grain sizes are shown in the micrographs of the unfatigued and fatigued samples due to an inhomogeneous grain size distribution in the polycrystalline materials. No significant differences are visible between the fracture surfaces of the virgin and fatigued samples, as shown in Fig. 9. Both samples exhibit mainly an intergranular fracture mode with rare transgranularly fractured grains.

IV. DISCUSSION

A. Switching mechanism and fatigue state

The strain and polarization hysteresis loops for the virgin samples in Figs. 1(a) and 3(a) are typical for antiferroelectric ceramics, showing a normal AFE-FE phase transition with a sudden increase in field induced strain and polarization at E_{AF}. In the virgin state, columns of ions in the antiferroelectric crystals are spontaneously polarized, but with neighboring columns polarized in antiparallel directions.[26] The mate-

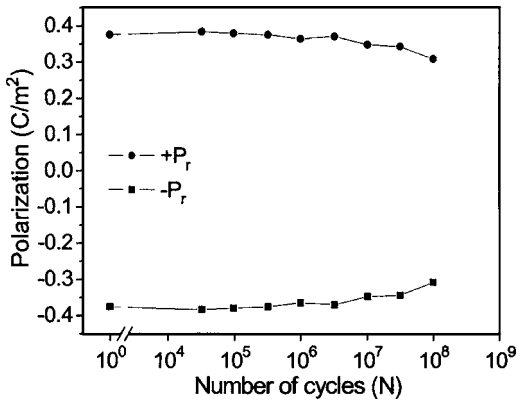

FIG. 4. Switchable polarization of the polarization hysteresis loop as a function of cycling.

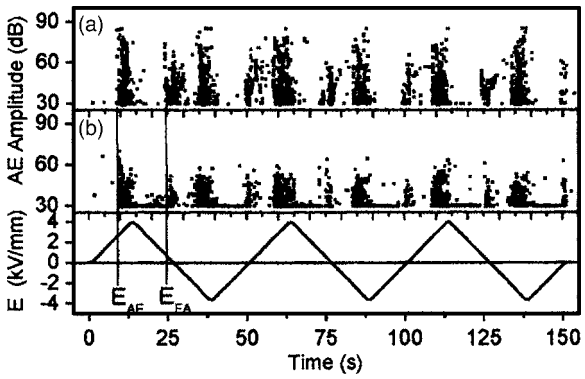

FIG. 6. AE patterns as a function of time in three measurement cycles for the samples in (a) the virgin state and (b) the fatigued state (cycled at 4 kV/mm, 50 Hz for 10^8 cycles).

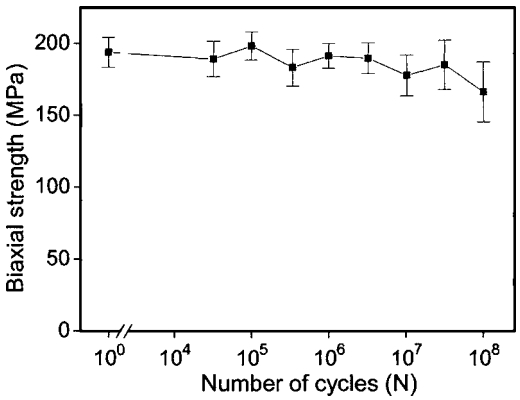

FIG. 7. Biaxial strength of the material as a function of cycling.

rial thus exhibits no macroscopic polarization. As the free energy of the antiferroelectric is close to that of the ferroelectric form of the material, the transition from the antipolar to polar dipole ordering can be driven by high electric field. The AFE-FE transition is accompanied by a large jump in the unit cell volume and a large macroscopic longitudinal extension resulting from the unit cell expansion component along the direction of the applied field. The transition from the antiferroelectric to the ferroelectric state also results in field induced macroscopic polarization. The material shows an abrupt AFE-FE phase transition at a critical electric field (E_{AF}), whereas the FE-AFE back transition proceeds over a more extended interval. The mechanism for the further increase in strain and polarization beyond the transition is still not well known. It is assumed that after E_{AF} is exceeded further expansion of the material is determined by nucleation of the FE phase, reverse piezoeffect, and 109° and 71° domain reorientations. While further increase in polarization depends on nucleation of the FE phase and domain reorientation under the applied field.[4] The material does not behave exactly electrostrictive, with a deviation of $S=f(P^2)$ (Landau-Devonshire theory) from linearity, especially at E_{AF}.

The material shows significant fatigue effects from 10^6 cycles. The switchable polarization decreases down to 10% of the original value at 10^8 cycles, with 23% and 28% loss of S_l and S_r, respectively. The deterioration of the properties in the antiferroelectric PZST ceramics is much less than in the ferroelectric PZT cycled at 50 Hz with lower cycling field,[11] indicating a higher fatigue resistance of the AFE material. Ferroelectric bulk materials and thin films show four fatigue stages when the cycle number reaches to 10^8.[4,11,21] According to the degradation of the properties with the cycle number, the antiferroelectric fatigue in this study undergoes the stages from the incubation to the logarithmic period or, at most, to a saturation state since there is no indication of recovery of the properties till 10^8 cycles.

B. Microcracking, etch grooves, and mechanical strength

Microcracking is a common and inevitable process in ferroelectric and antiferroelectric materials under cyclic electric or electromechanical loadings.[8,18,27–30] The large strain

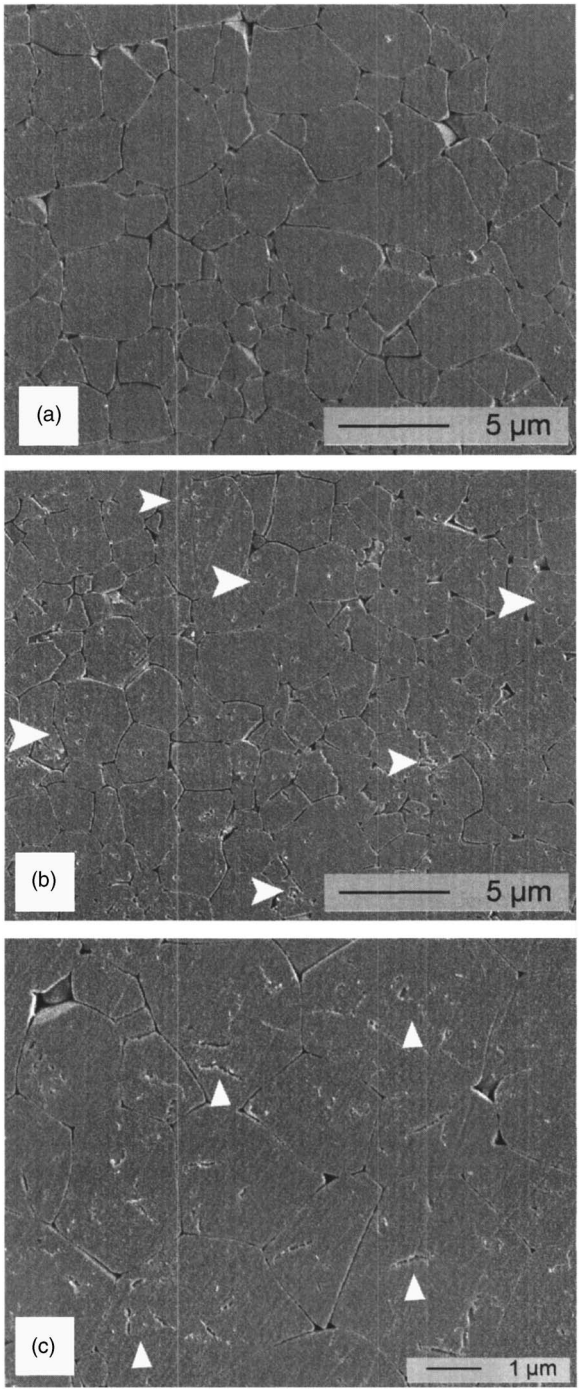

FIG. 8. Micrograph of the unfatigued material (a) and the material cycled at 4 kV/mm, 50 Hz for 10^8 cycles [(b) at low magnification and (c) at high magnification].

($>10^{-3}$) in ferroelectric and antiferroelectric materials induced by high electric fields is near the failure deformation ($\sim 10^{-3}$) in conventional ceramics.[29] The piezoelectric and electrostrictive coefficients are anisotropic and therefore electrically induced stress causes nonuniform deformation depending upon different orientations of the grains. In polycrystalline materials, each grain is surrounded by other grains that have different crystallographic orientations; the orientation mismatch of grains can give rise to incompatible deformation when a large electric field is applied, which in turn generates internal stress between individual grains.

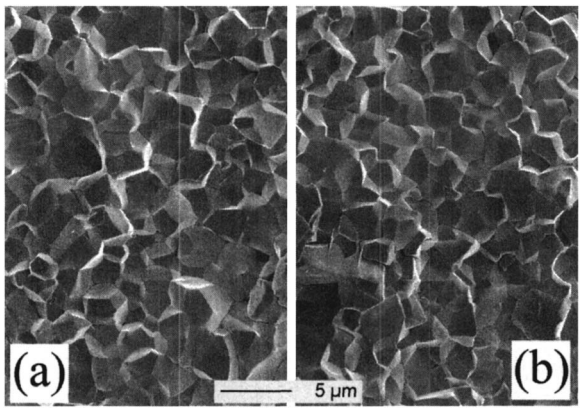

FIG. 9. Micrographs of fracture surfaces of the unfatigued material (a) and the material cycled at 4 kV/mm, 50 Hz for 10^8 cycles (b).

When these stresses exceed a certain value, microcracking takes place in the brittle solids to relieve the strain energy.[29] By the use of optical microscopy (OM) and SEM, the invisibility of microcracks in the present material indicates a weak microcracking during cycling.

One should distinguish the microcracks from the etch grooves observed in Figs. 8(b) and 8(c). The microcracks are generated under high internal stress and distributed along grain boundaries.[3,4,8,29,30] Those cracks can be observed at least by transmission electron microscopy (TEM) without any further treatment[27,28] and by SEM and OM when microcrack clouds and macrocracks develop.[8,18,29] The etch grooves can only be observed by SEM after acid etching and are distributed mainly within grains. In the antiferroelectric material studied previously, microcrack clouds and macrocracks can be observed by OM, indicating severe microcracking during electric cycling. Nevertheless, no etch grooves were detected by SEM in the fatigued samples.[8] In the present material, microcracking was so weak that microcrack clouds and macrocracks did not develop when the cycle number was up to 10^8. The resultant microcracks are actually invisible under OM and SEM. Numerous etch grooves, however, can be detected within grains after acid etching.

It is evident that the etch grooves do not contribute to the decrease in mechanical strength of the material since those grooves are distributed within grains and the microstructure of fracture surfaces of the fatigued samples shows the same intergranular fracture mode as that of the virgin samples. Microcracking during the electric cycling is therefore confined to materials which exhibit degradation of the biaxial strength, however, the data show that the influence of the microcracks on this property is not pronounced. Concerning the reduction of biaxial strength the material exhibits high resistance to electric cycling.

C. Fatigue mechanism and the pinning effect

The fatigue effect in the mechanical strength is a result of microcracking during electric cycling. The fatigue effect in the strain and polarization hysteresis loops, however, cannot be attributed to microcracking mainly. Fatigue cracks develop in cofired ceramic multilayer actuators around electrode edges with no significant changes of the properties.[31–33] In the present material, those properties are nearly fully recovered to their virgin state after heat treatment together with the diffuse AFE-FE phase transition and asymmetry of the wings of the strain hysteresis loop, indicating a dominant role of the pinning of domain walls as fatigue mechanism. The pinning of domain walls is a general accepted fatigue mechanism for ferroelectric materials.[11] The present fatigued material shows similar etch grooves as previously observed in ferroelectric PZT materials after bipolar electric and electromechanical cyclings.[10,11] These grooves indicate a cluster growth of point defects, resulting in the corrosion paths that react differently to the acid attack than the surrounding bulk material. Clusters of point defects were also observed as sources of the pinning effect by atomic force microscope (ATM) in ferroelectric PZT bulk material.[34] For the present antiferroelectric material, it is evident that the point defect agglomerations result in the pinning of both ferroelectric and antiferroelectric domain walls, which serves as the main fatigue mechanism.

There are alternative scenarios for the asymmetric degradation of the strain hysteresis due to electric cycling in ferroelectric materials. One is related to a preferred poling directions;[35–37] the second is attributed to the existence of a unidirectional frozen polarization or offset polarization as a result of the pinning of ferroelectric domain walls in a preferential direction.[10,11,38–40] The hypothesis of offset polarization is consistent with the observation of special regions with a strong preferential direction of the frozen polarization domains by AFM.[41] Since there is no preferential orientation of domains in the virgin samples before cycling, the former hypothesis is excluded for the antiferroelectric ceramics. The pinning of ferroelectric domain walls in a preferential direction is assigned as the source of strain hysteresis asymmetry. Antiferroelectric domains show no polarization and offset polarization. Calculation of the value of offset polarization was attempted for a commercial PZT ferroelectric material (PIC 151, PI Ceramic, Lederhose, Germany) according to the Landau-Devonshire theory,[11,39] assuming that the strain of the material is proportional to the square of the total polarization, which is not the case for the antiferroelectric PZST material, especially at E_{AF}.

The diffuse AFE-FE phase transition due to the electric cycling can be easily interpreted by the pinning of antiferroelectric domain walls. After a period of cycling, the accumulated point defect agglomerates are able to sufficiently clamp antiferroelectric domain walls. Thus a higher energy, i.e., a higher electric field is needed to excite the AFE-FE phase transition. The energy needed for the phase transition of individual domains is distributed over a range of electric fields and, thus, results in the diffuse phase transition. A small fraction of remaining ferroelectric phase in antiferroelectric matrix may serve as nuclei for the new ferroelectric phase and contribute to the diffuse phase transition.

It is evident that the diffuse character of AFE-FE phase transition protected the present material from being damaged by severe cracking that is the case for the material reported in Ref. 8. The previous material showed a normal character of AFE-FE phase transition, taking place at a critical electric field and resulting a sudden large stress accompanied by a

severe cracking. The phase transition in the present material occurs gradually within a range of electric field, which is assumed to induce much more lightly cracking. Thus, the present material shows no noticeable micro- or macrocracks after electric cycling in contrast to numerous macrocrack and microcrack clouds in the previous material.

D. Acoustic emission

In the virgin antiferroelectric PZST ceramics, numerous AE events occur only around E_{AF} and E_{FA}, and in the field range from E_{AF} to E_{max}. It is evident that the dominant AE sources in the material are the AFE-FE and FE-AFE phase transitions. The nucleation of domains is the AE source for phase transition in ferroelectrics.[42] In the antiferroelectric PZST ceramics, the nucleation of FE domains from AFE matrix and AFE domains from FE matrix is involved as AE sources. In the field range from E_{AF} to E_{max}, the nucleation of FE domains and discontinuous switching of FE domains clamped by some obstacles at high strain state are the most probable AE sources. Discontinuous domain switching is common as the AE source in ferroelectric phases.[24] Microcracking is also a likely AE source in the material since the microcracking process is inevitable in the ceramics. As discussed above, the microcracking process in the material is weak and is excluded as a dominant AE source, since there are no defects observed, by OM and SEM, in the material suffered 10^8 cycles. A detailed discussion of acoustic emission and the relevant sources under bipolar electric driving is the subject of another paper for antiferroelectric $Pb_{0.97}La_{0.02}(Zr_{0.77}Sn_{0.14}Ti_{0.09})O_3$ ceramics with fine and coarse grain sizes.

The AE patterns in the antiferroelectric PZST material are the same in the virgin and fatigued samples except the amplitudes of the AE events. AE events occur only around the transition fields and the field range from E_{AF} to E_{max} irrespective of the cycle number, while the maximum and average amplitudes of AE hits in a measuring cycle decrease with cycle number. This is in contrast to those results for ferroelectric PZT ceramics, where AE patterns change with electric cycling.[11] The maximum AE amplitude increases, while the threshold electric field decreases with number of cycles. The modification of AE pattern in PZT is attributed to the hindrance of domain wall motion by some obstacles sufficiently large to generate an acoustic pulse of noticeable energy. The domain must still be mobile to some extent, i.e., once the energy barrier is too high for overriding a particular obstacle, the domains become entirely clamped and thus no longer contribute to the observed AE. In the antiferroelectric PZST ceramics, since there is no domain switching for the rising field below E_{AF}, no AE events occur in this field range. At E_{AF} and E_{FA}, as well as in the field range between E_{AF} and E_{max}, AE events resulting from the hindrance of domain wall motion may occur. These AE events, however, cannot be distinguished from those for normal discontinuous domain switching. The AE patterns for unfatigued and fatigued materials are thus the same.

For the antiferroelectric PZST, the reduction in the amplitude of AE events in fatigued samples during a measuring cycle can be explained by considering two aspects. One is that when the material exhibits diffuse phase transition and pinning effect with smaller and slower microscopic strain changes, as well as a smaller total strain due to cycling, the nucleation of new domains and discontinuous domain switching will take place at lower strain and stress, thus generating AE events with low energies and amplitudes. The other scenarios are related to the microstructure modification in the materials due to the electric cycling. The phase and domain switching is more difficult in the original state of the configuration and is accompanied with a delivery of higher energy, yielding louder acoustic emission. The configuration is modified with cycling, which makes the switching more and more easy. After a certain number of cycles, the material becomes textured by the driving electric field. The switching then goes more smoothly, generating lower acoustic emission. The mechanism is similar to AE occurring at the morphtropic phase boundary composition of PZT.[24] These two processes may act as a combined contribution to the reduction in the amplitude of AE events for fatigued materials.

V. SUMMARY

The antiferroelectric PZST material shows a high fatigue resistance to bipolar electric cycling concerning the losses in the macroscopic properties as well as the modification of microstructure. At 10^8 cycles, the decreases in biaxial strength, maximum strain of the left and the right part of strain hysteresis loop, and switchable polarization are 15%, 23%, 28%, and 10% of the initial values, respectively. The degradation in the mechanical strength is assigned to fatigue microcracking which is comparatively weak in the present antiferroelectric material. The pinning of domains by point defect agglomeration is discussed as the dominant fatigue mechanism for the fatigue effects in field induced strain and polarization as well as for a diffuse antiferroelectric to ferroelectric phase transition. The asymmetry of the strain hysteresis loop for the fatigued material is attributed to offset polarization resulting from a preferential direction of the pinning of the field forced ferroelectric domains.

ACKNOWLEDGMENTS

The authors gratefully acknowledge financial support by the Deutsche Forschungsgemeinschaft. R. Mager's help in technical support is cordially appreciated.

[1] B. Wu, Y. Ye, Q. Wang, and L. E. Cross, J. Appl. Phys. **85**, 3753 (1999).
[2] W. Pan, Q. Zhang, A. Bhalla, and L. E. Cross, J. Am. Ceram. Soc. **72**, 571 (1989).
[3] W. Pan, C. O. Dam, Q. M. Zhang, and L. E. Cross, J. Appl. Phys. **66**, 6014 (1989).
[4] L. Shebanov, M. Kusnetsov, and A. Sternberg, J. Appl. Phys. **76**, 4301 (1994).
[5] D. Berlincourt, H. H. A. Krueger, and B. Jaffe, J. Phys. Chem. Solids **25**, 659 (1964).
[6] B. Jaffe, Proc. IRE **49**, 1264 (1961).
[7] Q. Y. Jiang and L. E. Cross, J. Mater. Sci. **28**, 4536 (1993).
[8] L. Zhou, A. Zimmermann, Y. Zeng, and F. Aldinger, J. Am. Ceram. Soc. **87**, 1593 (2004).
[9] K. Takemura, M. Ozgul, V. Bornand, S. Trolier-Mckinstry, and C. A. Randall, J. Appl. Phys. **88**, 7272 (2000).
[10] D. C. Lupascu, E. Aulbach, and J. Rödel, J. Appl. Phys. **93**, 5551 (2003).
[11] J. Nuffer, D. C. Lupascu, and J. Rödel, Acta Mater. **48**, 3783 (2000).

[12]U. Robels, L. Schneider-Störmann, and G. Arlt, Ferroelectrics **168**, 301 (1995).
[13]C. Brennan, Ferroelectrics **150**, 199 (1993).
[14]A. K. Tagantsev and I. A. Stolichnov, Appl. Phys. Lett. **74**, 1326 (1999).
[15]Q. Y. Jiang, W. Cao, and L. E. Cross, J. Am. Ceram. Soc. **77**, 211 (1994).
[16]H. M. Duiker, P. D. Beale, J. F. Scott, C. A. Paz de Araujo, B. M. Milnick, J. D. Cuchiaro, and L. D. Mcmillan, J. Appl. Phys. **68**, 5783 (1990).
[17]J. Nuffer, D. C. Lupascu, and J. Rödel, Appl. Phys. Lett. **80**, 1049 (2002).
[18]Q. Y. Jiang, E. C. Subbarao, and L. E. Cross, J. Appl. Phys. **175**, 7433 (1994).
[19]J. H. Jang and K. H. Yoon, Jpn. J. Appl. Phys., Part 1 **37**, 5162 (1998).
[20]J. H. Jang, K. H. Yoon, and K. Y. Oh, Mater. Res. Bull. **35**, 393 (2000).
[21]E. L. Colla, A. K. Tagantsev, D. V. Taylor, and A. L. Kholin, Integr. Ferroelectr. **18**, 19 (1997).
[22]T. F. Drouillard, J. Acoust. Emiss. **14**, 1 (1996).
[23]*Proceedings of the International Conference on Acoustic Emission*, Anaheim, CA, 1979, edited by H. L. Dunegan and W. F. Hartman (Dunhart, Knoxville, TN, 1981).
[24]D. C. Lupascu and M. Hammer, Phys. Status Solidi A **191**, 643 (2002).
[25]A. Börger, P. Supancic, and R. Danzer, J. Eur. Ceram. Soc. **22**, 1425 (2002).
[26]C. Kittel, Phys. Rev. **82**, 729 (1951).
[27]G. S. White, A. S. Raynes, M. D. Vaudin, and S. W. Freiman, J. Am. Ceram. Soc. **77**, 2603 (1994).
[28]M. D. Hill, G. S. White, and C. Hwang, J. Am. Ceram. Soc. **79**, 1915 (1996).
[29]Q. Y. Jiang, E. C. Subbarao, and L. E. Cross, Acta Metall. Mater. **42**, 3687 (1994).
[30]H. Makino and N. Kamiya, Jpn. J. Appl. Phys., Part 1 **37**, 5301 (1998).
[31]S. Takahashi, A. Ochi, M. Yonezawa, T. Yano, T. Hamatsuki, and I. Fukui, Ferroelectrics **50**, 181 (1993).
[32]S. Takahashi, Ceram. Bull. **65**, 1156 (1986).
[33]S. L. S. Lucato, D. C. Lupascu, M. Kamlah, J. Rödel, and C. S. Lynch, Acta Mater. **49**, 2751 (2001).
[34]D. C. Lupascu and U. Rabe, Phys. Rev. Lett. **89**, 187601 (2002).
[35]W. L. Warren, B. A. Tuttle, and D. Dimos, Appl. Phys. Lett. **67**, 1426 (1995).
[36]W. L. Warren, D. Dimos, B. A. Tuttle, G. E. Pike, and H. N. Al-Shareef, Integr. Ferroelectr. **16**, 77 (1997).
[37]H. Weitzing, G. A. Schneider, J. Steffens, M. Hammer, and M. J. Hoffmann, J. Eur. Ceram. Soc. **19**, 1333 (1999).
[38]A. L. Kholkin, E. L. Colla, A. K. Tagantsev, D. V. Taylor, and N. Setter, Appl. Phys. Lett. **68**, 2577 (1996).
[39]C. Verdier, D. C. Lupascu, and J. Rödel, J. Eur. Ceram. Soc. **23**, 1409 (2003).
[40]M. Ozgul, S. Trolier-McKinstry, and C. A. Randall, J. Appl. Phys. **95**, 4296 (2004).
[41]E. L. Colla, H. Seungbum, D. V. Taylor, A. K. Tagantsev, N. Setter, and N. Kwangsoo, Appl. Phys. Lett. **72**, 2763 (1998).
[42]E. A. Dul'kin, V. G. Gavrilyachenko, and A. F. Semenchev, Phys. Solid State **35**, 1016 (1993).